Article

Magnetic and Transport Anomalies and Large Magnetocaloric Effect in Cubic R_4PtAl (R = Ho and Er)

Kartik K. Iyer [1,2,*], Sudhindra Rayaprol [3], Ram Kumar [1,4], Shidaling Matteppanavar [5], Suneel Dodamani [2], Kalobaran Maiti [1] and Echur V. Sampathkumaran [6,*]

1   Tata Institute of Fundamental Research, Homi Bhabha Road, Colaba, Mumbai 400005, India
2   KLE Society's Dr. Prabhakar Kore Basic Science Research Centre, KLE Academy of Higher Education and Research, Belagavi 590010, India
3   UGC-DAE-Consortium for Scientific Research—Mumbai Centre, BARC Campus, Trombay, Mumbai 400085, India
4   Maryland Quantum Materials Center and Department of Physics, University of Maryland, College Park, MD 20742, USA
5   KLE Society's Basavaprabhu Kore Arts, Science & Commerce College, Chikodi 591201, India
6   Homi Bhabha Centre for Science Education, TIFR, V. N. Purav Marg, Mumbai 400088, India
*   Correspondence: iyer@tifr.res.in (K.K.I.); sampathev@gmail.com (E.V.S.); Tel.: +91-22-22782439 (K.K.I.)

Abstract: We report the electronic properties of R_4PtAl (R = Ho, and Er), which contains three sites for R, by the measurements of magnetization (ac and dc), heat-capacity, transport, and magnetoresistance (MR). Dc magnetization data reveal antiferromagnetic order below 19 K and 12 K in Ho and Er compounds, respectively. Additional features observed at lower temperatures (12 K for Ho$_4$PtAl and 5 K for Er$_4$PtAl) are akin to the cluster spin-glass phase. Resistivity data exhibit a weak minimum at a temperature marginally higher than their respective Néel temperature (T_N), which is unusual for such rare-earths with well-localized 4f states. Isothermal magnetization and magnetoresistance data well below T_N exhibit signatures of a subtle field-induced magnetic transition for a small magnetic field (<10 kOe). Notably, the isothermal entropy change at T_N has the largest peak value within this rare-earth family; for a field change from zero to 50 kOe, the entropy change is ~14.5 J/kg K (Ho4PtAl) and ~21.5 J/kg K (Er$_4$PtAl) suggesting a role of anisotropy of 4f orbital in determining this large value. The results provide some clues for the advancement of the field of magnetocaloric effect. The magnetocaloric property of Er$_4$PtAl is nonhysteretic, meeting a challenge to find materials with reversible magnetocaloric effect.

Keywords: rare earth intermetallics; magnetocaloric effect; antiferromagnetism

1. Introduction

There is a general consensus that the technology of "magnetic refrigeration" can increase the efficiency of cooling when compared to the conventional gas-compression route. Therefore, there are constant efforts in the current literature to find clues to improve the magnetocaloric effect (MCE) as well as to discover new solid materials which are cost-efficient, as well as those that minimize the problems due to irreversibility in magnetic-field (H) cycling. Gd metal, being a large magnetic-moment element, seems to remain the benchmark for applications, even after several decades of intense research. It is needless to emphasize that the exceptional MCE behavior of Gd$_5$Si$_2$Ge$_2$ reported by Pecharsky and Gschneidner [1] in 1997 has been at the centerstage of the field of MCE, but its application has been limited due to the hysteretic nature of the first-order magnetic-field induced magnetic transition. Naturally, the search for new rare-earth (R) compounds with magnetic anomalies continues to be an important direction of research to find favorable MCE materials in different temperature (T) ranges. Keeping this scenario in mind, we have investigated the magnetic and MCE behavior of two rare-earth compounds, R_4PtAl (R = Ho and Er).

The compounds of the type R_4TX (T = transition metals and X = p-block metal) with the cubic Gd_4RhIn-type structure [2–5] provide a new platform in the field of "frustrated magnetism", as multiple sites for R seem to favor a spin-glass state, competing with antiferromagnetism (AF) and ferromagnetism (F) [6–11]. The crystal structure is shown in Figure 1 to bring out the surrounding of the three R ions. Complexities of crystallography for this family have been discussed by Engelbert and Janka in the literature [5] and also presented in our earlier publication [7].
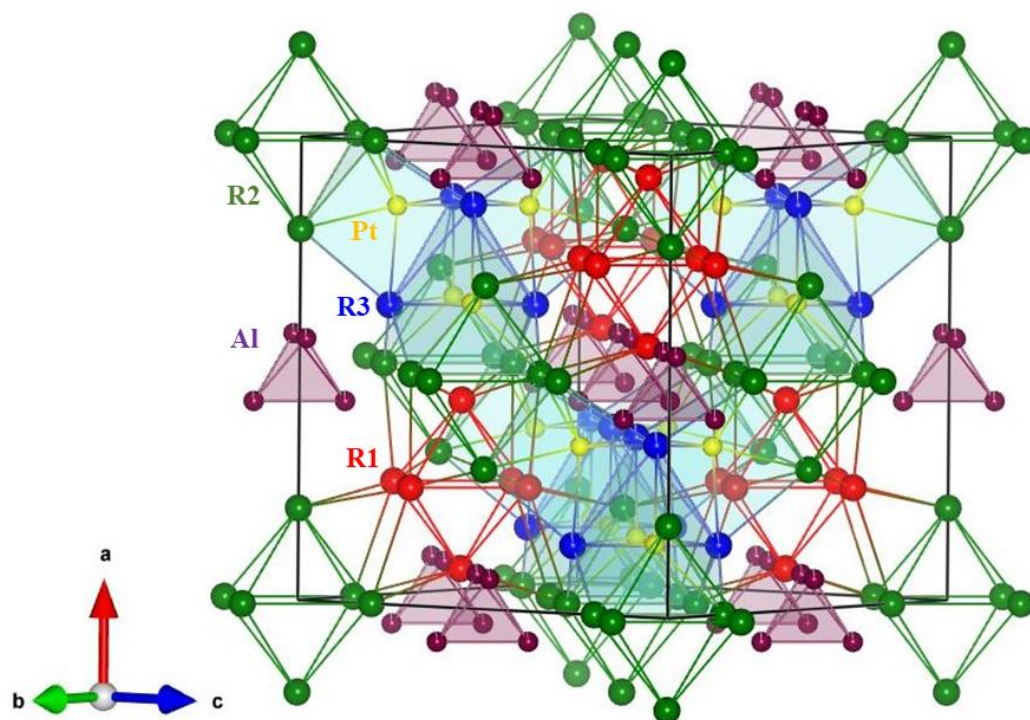

Figure 1. Crystal structure of R_4PtAl (R = Rare-earth). The rare-earths with different chemical environments can be seen. The rare-earths $R1$ (red) and $R2$ (green) form separate octahedra and $R2$ and $R3$ form an octahedra with Pt (yellow) at the center. The rare-earth $R3$ (blue) forms a tetrahedra. Al forms a tetrahedra.

Recent investigations on some members of this class of compounds have established that there are novel transport anomalies, not only in the magnetically ordered state, but also in the paramagnetic state [6–11]. Here, we focus on the heavy R members of the Pt-based family, R_4PtAl, where the $4f$ states are far away from the Fermi level (thereby avoiding the complex, well-known phenomena due to $4f$-hybridization in light rare-earths); Pt $5d$ electrons are expected to be weakly correlated, although possessing strong spin-orbit coupling. Extensive studies in recent years revealed that Gd_4PtAl shows re-entrant spin-glass behavior around 20 K below its Néel temperature (T_N = 64 K) [6], whereas Tb_4PtAl exhibits spin-glass features at the onset of the AF order at 50 K and an additional spin-glass anomaly at a further lower temperature [7]. Curiously, the Dy analogue undergoes a ferromagnetic transition at (T_C=) 32.6 K, indicating an unusual role of Pt $5d$ states on the magnetism of a rare-earth with well-localized $4f$ orbital [11], which transforms to a spin-glass phase around 20 K [8]. There are magnetic-field-induced features as well, attributable to first-order transitions in most of these compounds. The experimental results presented in this article on Ho and Er compounds reveal fascinating magnetic and transport anomalies with an exceptional MCE, as inferred from the values of the isothermal entropy change (ΔS), in comparison with the values reported earlier for this family; this finding at low-temperatures provides some clues for further theoretical advancement in the field of MCE to enable the discovery of new materials for room temperature applications.

2. Materials and Methods

Samples were prepared in polycrystalline form by arc-melting stoichiometric amounts of constituent elements in an argon atmosphere. The Er compound needed to be annealed at 650 °C for 8 days. Powder x-ray diffraction patterns (XRD), shown in Figure 2, were obtained using Cu-Kα radiation, and these were found to be in good agreement with those reported in Ref. [5]. Rietveld refinement further helped in understanding the diffraction patterns. Such an analysis enabled us to ascertain the formation of the cubic phase with the space group $F\bar{4}3m$. It may be mentioned that the XRD pattern showed a weak extra line around 36° for the unannealed Er sample, which disappeared after annealing. Scanning electron microscopic images revealed the homogeneity of the samples without showing any extra phase. Dc magnetic susceptibility (χ) (1.8 to 300 K) and isothermal magnetization (M) measurements were performed with the help of a commercial (Quantum Design) superconducting quantum interference device; ac χ data were also collected in a T-region of interest with an ac field of 1 Oe with different frequencies (v = 1.3, 13 and 133 Hz) with the same magnetometer. Heat-capacity (C) and electrical resistivity (ϱ) and magnetoresistance (MR) measurements down to 1.8 K and also as a function of H were caried out using a commercial (Quantum Design Physical Property Measurement System). Unless otherwise stated, all the measurements were performed for the zero-field-cooled (ZFC) condition of the specimens.
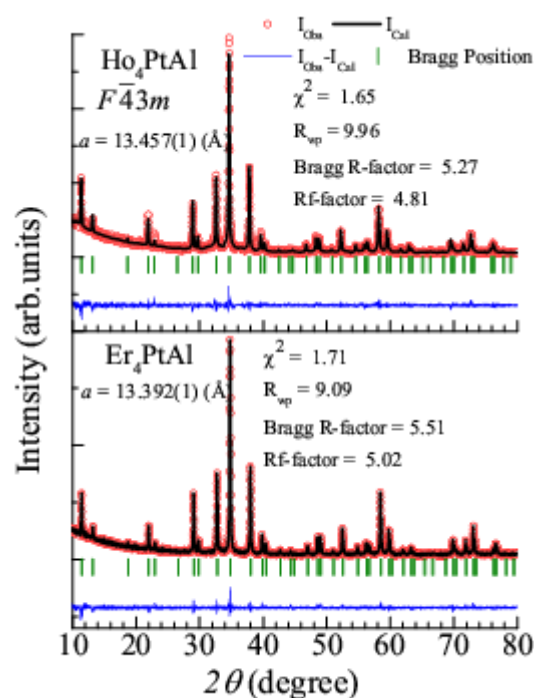

Figure 2. X-ray diffraction patterns of Ho$_4$PtAl and Er$_4$PtAl at room temperature, along with Rietveld fitting results.

3. Results and Discussions

Figures 3a,b and 4a,b show χ(T) measured in 5 kOe magnetic field as well as in 100 Oe field for both the samples. Inverse χ, plotted for 5 kOe data in the mainframe, is linear above 50 K.
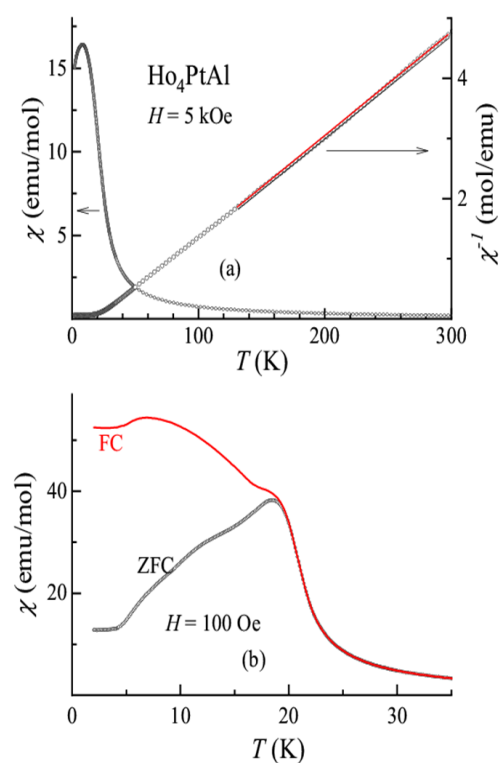
Figure 3. The temperature-dependent dc magnetic susceptibility and inverse susceptibility for Ho_4PtAl, measured in (**a**) 5 kOe and (**b**) 100 Oe. In (**b**), the curve obtained for field-cooled warming conditions is also included. In (**a**), a straight line in the inverse χ plot above 120 K represents Curie–Weiss fitting.
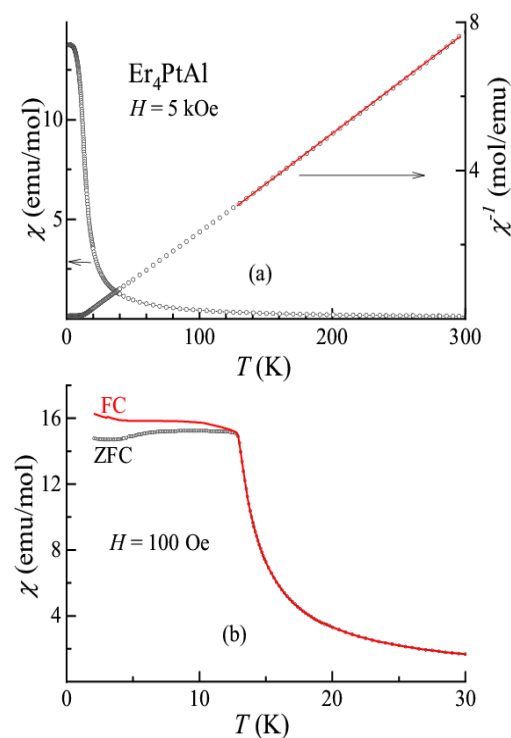

Figure 4. The temperature-dependent dc magnetic susceptibility and inverse susceptibility for Er_4PtAl, respectively, measured in (**a**) 5 kOe and (**b**) 100 Oe. In (**b**), the curve obtained for field-cooled warming conditions is also included. In (**a**), a straight line in the inverse χ plot above 120 K represents Curie–Weiss fitting.

The values of the effective magnetic moments (~10.7 μ_B and 9.82 μ_B per Ho and Er, respectively) derived from the high-temperature paramagnetic region are in good agreement with the theoretical values (10.6 and 9.59 μ_B, respectively) (see, for instance, Ref. [12]). The corresponding values of paramagnetic Curie temperature (θ_p) are ~27 K and 16 K. The positive sign of θ_p indicates that ferromagnetic coupling between the rare-earth moments is dominant in these compounds in the Curie–Weiss regime, as also observed in the cases of Gd, Tb, and Dy members [6–8]; the situation is more complex at lower temperatures as described below. For the Ho compound, as the T is lowered, there is a peak in $\chi(T)$ in the ZFC curve for H = 100 Oe near 19 K (Figure 3b) attributable to the long range antiferromagnetic order, followed by a shoulder near 12 K and a flattening below about 5 K, as though there are additional magnetic transitions. The ZFC curve obtained in 5 kOe field smeared out these additional magnetic features. This suggests that the magnetism is sensitive to external magnetic fields. Irreversibility appeared in the 100 Oe field-cooled (FC) and ZFC curves (Figure 3b) at around 19 K, signaling a possibility of the spin-glass phase, though other factors (like domain wall boundary effects) have also been known to result in such a feature in ferromagnetic and antiferromagnetic materials. In the case of the Er sample, the features appear similar with magnetic ordering (presumably of an AF type, vide infra) setting in at 12 K along with an additional feature (a change of slope) around 5 K for the curves measured in 100 Oe (Figure 4b); the bifurcation of the low-field ZFC-FC curves in the magnetically ordered state can be seen even for this compound at around 12 K. It is important to note that the FC curves in both the cases tended to show an increase with decreasing temperature (though it is weak for the Er case) below T_N, which is a signature of cluster spin-glass behavior [6,13–15]. The observed values of magnetic ordering temperatures and θ_p are marginally higher compared to the respective de Gennes scaled values (for full degeneracy), as inferred from the knowledge of the corresponding values (64 K and 86 K) for the Gd analogue [6]. This means that anisotropy of the crystal-field-split 4f orbital probably plays a role in such a breakdown [16–18].

In Figure 5a,b, we show the $M(H)$ curves up to 70 kOe at selected temperatures in the magnetically ordered state for both compounds. The points to be noted are: (i) in these curves, there was a sharp increase of M for initial applications of H, indicating a possible tendency towards ferromagnetic alignment at a small H; there is a distinct step around 5 kOe for the Ho compound at 2 K in support of the fact that the zero-field state cannot be classified as a ferromagnet, but as a canted antiferromagnet undergoing spin reorientation; (ii) even at fields as high as 70 kOe, there is no evidence for saturation, supporting further the canted nature of magnetic structure persisting at high fields; (iii) distinct hysteresis, though weak, is observed for the Ho compound at 2 K, which was found to diminish gradually with increasing temperature well below T_N, as shown in Figure 4c for 16 K, in the low-field hysteresis measurements; this hysteresis suggests the existence of a ferromagnetic component; (iv) hysteresis is absent in the $M(H)$ curves for the Er compound down to 2 K (Figure 5d). The results overall suggest the canted antiferromagnetic nature of the virgin state at the onset of magnetic order.

We have measured ac χ to get more insight into the nature of the magnetically ordered state, given that the sign of θ_p positively supports the existence of ferromagnetic correlations, whereas the virgin specimens reveal the onset of antiferromagnetic order (as discussed above). The real (χ') and imaginary (χ'') parts are shown in Figure 6. In the case of Ho compound, χ' (in zero field) exhibits a peak at 19 K, followed by a shoulder around 12 K; there are upturns at similar temperatures in the χ''. No feature could be clearly resolved around 5 K, though χ'' exhibits a change of slope. All these features vanish in an applied field of 5 kOe, clearly revealing the existence of a spin-glass component. The υ-dependence of the peak, though weak, is discernable; the fact that it is seen even at the onset of long-range magnetic order does not rule out the possibility of antiferromagnetic cluster spin-glass behavior. In the case of Er compound, χ' (in zero field) exhibits a peak at ~12 K, followed by a distinct change of slope around 5 K, consistent with the dc χ data presented above. There is also a shoulder around 10 K, the origin of which is not clear; pos-

sibly, there is an additional spin-reorientation at this temperature, which is subtly sensitive to small fields, escaping detection in the dc χ measurements even in fields as low as 100 Oe. It appears that such subtle additional magnetic features could be observed under favorable circumstances due to complex interaction between the three non-equivalent magnetic sites, as also observed for the Tb analogue [7]. The frequency dependence of the peak is not well resolved, though the left side of the peak shows some dependence. However, the χ'' curves reveal a distinct frequency-dependent peak at about 5 K without any notable peak at higher temperatures. These findings imply that the 5 K-feature alone could arise from spin-glass freezing. An application of a dc magnetic field of 5 kOe completely suppresses the peaks. Viewing together with the behavior of low-field dc χ curves and dc M, we conclude that (virgin state) antiferromagnetism below 5 K behaves like (cluster) spin-glasses for the Er case.
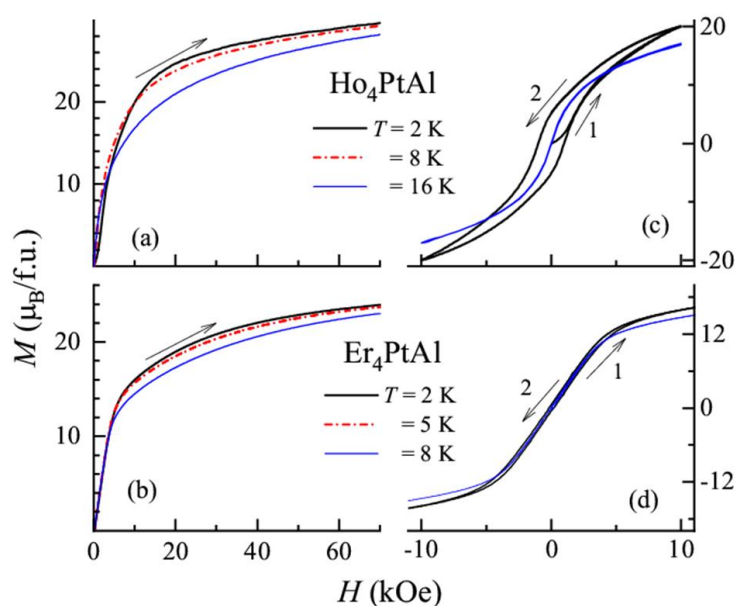

Figure 5. Isothermal magnetization (per formula unit) at selected temperatures for (**a**) Ho$_4$PtAl and (**b**) Er$_4$PtAl. In (**c**,**d**), respective low-field (0 to 10 to -10 to 10 kOe) hysteresis loops are shown for two temperatures.

In order to render support to the above conclusions for both the materials, we have measured isothermal remanent magnetization (M_{IRM}) at selected temperatures below T$_N$; for this purpose, we cooled the samples in 5 kOe to desired temperatures, switched off the field and measured M$_{IRM}$ as a function of time. It is noted (Figure 6e,f) that the value M_{IRM}, measured immediately after the field was switched off (labeled $M(0)$), decreases with the increase of T and also decreases slowly with time. Though the functional form of the decay with time appears to be complicated (e.g., two logarithmic regions are seen in Figure 6e,f), possibly due to the presence of multiple sites for R, the slow decay is consistent with the glassy behavior, at least in the close vicinity of 5 K for both the cases.

Figure 7 shows heat-capacity as a function of temperature for both the compounds in the form of C versus T as well as of C/T versus T below 40 K. It is clear that there is a well-defined feature (upturn followed by a peak) as the magnetic ordering temperature is approached from the paramagnetic state for both the compounds in the absence of a magnetic field. Additionally, for the Ho compound, there is a shoulder around 12 K in the plot of $C(T)$ (Figure 7a), which is more transparent in the plot of $C(T)/(T)$ (Figure 7b). There is also a weak upturn in C(T) below about 5 K, and it is possible that it *is* due to subtle changes in the orientation of magnetic moments. As the magnetic field *is* applied, for $H = 10$ kOe, the peak temperature is marginally decreased with the feature due to the onset of magnetic order partly overlapping with the one due to 12 K transition. This established that the magnetic structure at the onset of magnetic order is of an AF type and not of an

F-type as proposed earlier [5]. For further higher fields (30 and 50 kOe), the peak is smeared and there was a monotonic decrease of C with T down to 5 K (Figure 7c). With respect to the Er case, it is clear that, following a sharp rise below 14 K, the peak appears around 12 K (in zero field). The C/T plot (Figure 7d) shows an additional sharp anomaly around 5 K in support of a magnetic feature around this temperature, as indicated by ac χ. Below 10 K, there is no evidence for $T^{3/2}$ or T^3 behavior, expected for ferromagnets/spin-glasses and antiferromagnets, respectively, thereby revealing that the magnetism is, in fact, quite complex. It is not clear whether a shoulder in C/T near 10 K can be correlated to the ac χ feature at this temperature (see above). The H-dependence of the magnetic feature is somewhat similar to that of the Ho case, and the downward shift of the peak with H is consistent with the AF ordering at the onset of the magnetic transition.
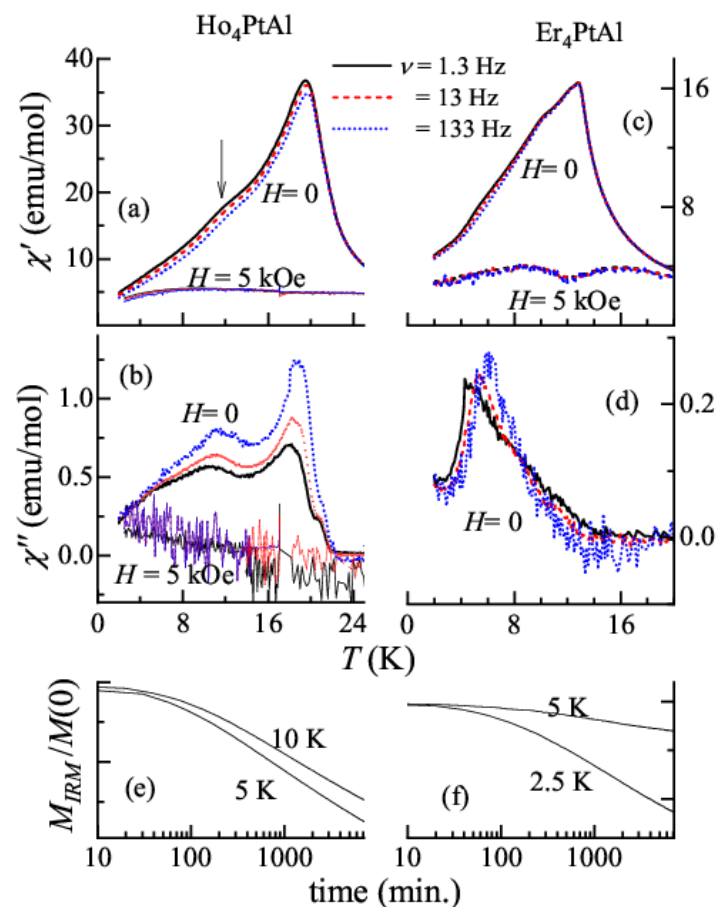

Figure 6. Real (χ') and imaginary (χ'') parts of ac susceptibility for Ho_4PtAl are shown in (**a**,**b**) and corresponding parts for Er_4PtAl are plotted in (**c**,**d**). A vertical arrow in (**a**) is drawn to show the temperature where the shoulder occurs. Time dependence of isothermal remnant magnetization at selected temperatures are plotted in (**e**) for the former and in (**f**) for the latter. In (**d**), the 5kOe-data is not plotted, as it is very noisy and featureless. The values of M_{IRM}, labeled $M(0)$, immediately after the field is switched off, are: For Ho, -14 and 6.3 emu/g for 5 and 10 K, and, for Er, 2.7 and 1.5 emu/g for 2.5 and 5 K, respectively.
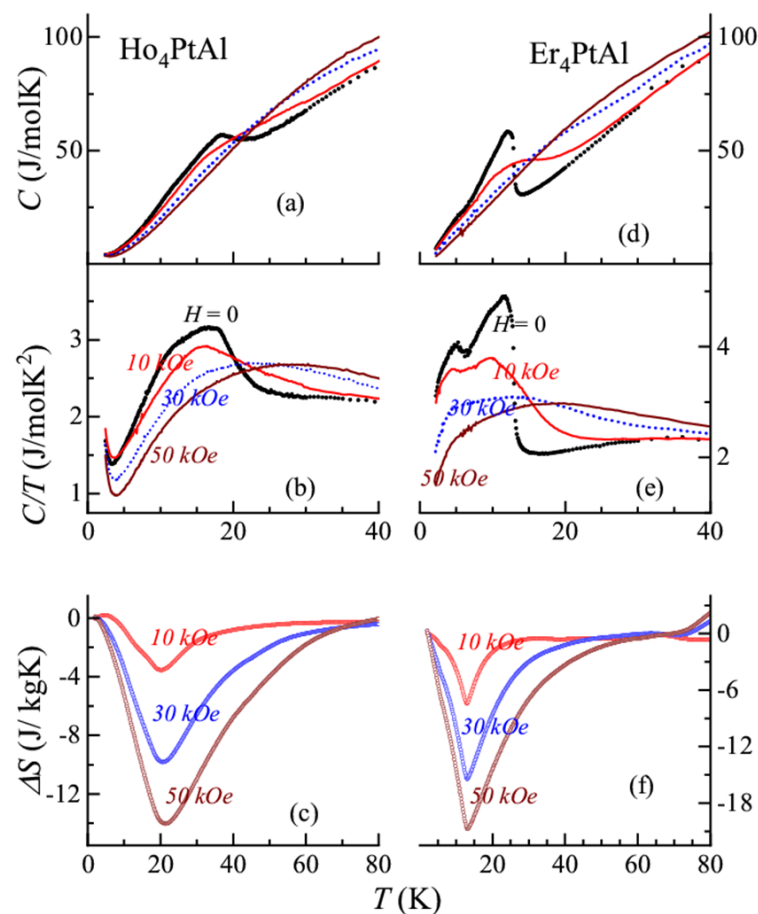
Figure 7. The plots of heat-capacity (*C*), heat-capacity divided by temperature, and isothermal entropy change (ΔS) as a function of temperature for Ho_4PtAl are shown in (**a**–**c**), respectively. Corresponding plots for Er_4PtAl are shown in (**d**–**f**).

We have derived isothermal entropy change, $\Delta S = S(H) - S(0)$, by integrating the plots of C/T, and the results obtained are shown in Figure 6c,f, for selected final fields. The plots of ΔS exhibit a peak in the negative quadrant for both cases, even for an application of a field as small as 10 kOe; this sign is typical of ferromagnetism [19] and, therefore, this supports the inference made from *M(H)* for the appearance of a ferromagnetic component even for such low fields (though AF component still persists as discussed above). We had also obtained ΔS from isothermal *M* data employing Maxwell's equation for the Er case by measuring isothermal *M* in close intervals of temperature (every 3 K, not shown here); the values and the features are in good agreement with that derived from the *C(T)* data. We would like to emphasize the following outcome: (i) the peak values of ΔS are relatively large for both the compounds, compared to that of analogous Gd, and Tb members [6–8]. For instance, for a field of 50 kOe, the values for Ho and Er members are about ~14.5 and ~21.5 J/kg K, whereas the corresponding values are lower for Gd (~6 J/kg K). For Tb and Dy cases, the corresponding peak values are ~ 6 and 13 J/kg K, respectively. Clearly, the value for the Er sample is the largest within this family. The magnetic refrigeration capacity, defined as the product of the full-width at half maximum and the peak value, is quite large—about 420 J/kg K—and comparable to many best magnetocaloric materials in this temperature range of interest [20]. This finding, therefore, reinforces [9] that the anisotropy of the (crystal-field-split) 4f orbital (that is, aspherical nature) plays a key role for such an enhancement. (ii) The peak values of these two Pt compounds are far higher than those of the respective member of the isomorphous Rh family as well [9–11]. In fact, a comparison of the peak values of ΔS between Pt and Rh families suggests that this is in general true for a given R, e.g., for Gd_4PtAl and Gd_4RhAl, the values are ~6 and ~2.3 J/kg K,

respectively [6,9]. It is known that the electronic correlation within the 4d bands is usually stronger than that within 5d bands in transition metal systems; on the other hand, the spin-orbit coupling is stronger for the latter. We, therefore, wonder spin-orbit coupling effect of the Pt 5d electrons plays a role in enhancing MCE. It is needless to elaborate that the correlated electrons in the event of stronger spin-orbit coupling (compared to crystal-field splitting and electron hopping amplitude) resulted in a rich variety of spin-orbit entangled phenomena, as demonstrated in recent years for oxide systems (see, for a review, Ref. [21]); (iii) as discussed for other compounds of this family [6,9–11], the plot of ΔS exhibits a long tail over a wide T-range above T_N, possibly arising from a gradual formation of ferromagnetic clusters with a lowering of temperature (behaving like a classical spin-liquid). The readers may note that interesting magnetic precursor effects have been brought out in different contexts, as well in the past, in insulting materials [22–25]. (iv) The isothermal magnetization curves were non-hysteretic for the Er case, and, in view of this, this compound can be added to the list of materials for magnetic refrigeration below 40 K, considering that it is often emphasized in the literature to find materials with such a reversible behavior [26,27].

The $\varrho(T)$, as expected for metals, exhibits a positive temperature coefficient as the temperature is lowered below 300 K (Figure 8a,b) but exhibits a minimum in the paramagnetic state just above the ordering temperature in both the cases in zero field (at 26 K and 14 K, respectively) (Figure 8c,d, insets). Such a minimum, though not expected for rare-earths with localized 4f electrons like Ho and Er, was encountered in some heavy rare-earth systems as a precursor to long-range magnetic order [10,28,29]. Recent new theoretical ideas attribute it to classical spin-liquid behavior due to geometrically frustrated magnetism [30]. Such a minimum vanished gradually with the application of an external magnetic field, as shown in Figure 8c,d, for an application of 10 kOe. As the material enters a magnetically ordered state, the drop due to the loss of spin-disorder contribution (see zero field curves) could be seen. Following interesting observations were made on the magnetoresistance (MR = $[\varrho(H) - \varrho(0)]/\varrho(0)$) data, even in the paramagnetic state (Figure 9). There was a competition between positive contribution due to the Lorentz motion of the conduction electrons (that is, classical metallic part, varying quadratically with H) and negative contribution due to the suppression of spin fluctuation contribution by H as a function of H and T. Thus, at 18 K (close to T_N), for the Er case, there was initially an increase in the positive quadrant due to metallic contribution, followed by a peak around 25 kOe and then a fall with the curve entering the negative quadrant around 55 kOe due to spins. At higher temperatures, say at 25 K, MR curve remains in the positive quadrant due to the weakening of spin contribution with respect to the metallic part. On the other hand, for the Ho compound, just above its T_N, say, at 25 K, the spin contribution dominated, as revealed by the negative sign, until about 25 kOe, and it was overcompensated at higher fields by the metallic part at higher fields. At higher temperatures, the MR(H) curve stays in the positive quadrant only. Concerning the behavior below T_N (Figure 10), the sign of MR remains negative, either due to antiferromagnetic gap formation and/or spin-glass component. The fact that the antiferromagnetic-gap formation occurs is evidenced, at least for the Ho case, by the observation that there was initially a (weak) upturn in ϱ (in the zero-field curve) as soon as the magnetically ordered state was entered; this upturn was suppressed by a field of 10 kOe (see Figure 8). A notable finding in the isothermal MR curves is that the virgin curve lay prominently outside the envelope loop below 12 K in the low-field range (<4 kOe) with a significant hysteresis for the Ho case, supporting that there could be a disorder-broadened first-order magnetic transition at such low fields; however, in the Er case, the magnitude of MR was so small that hysteresis MR(H) could be considered negligible.
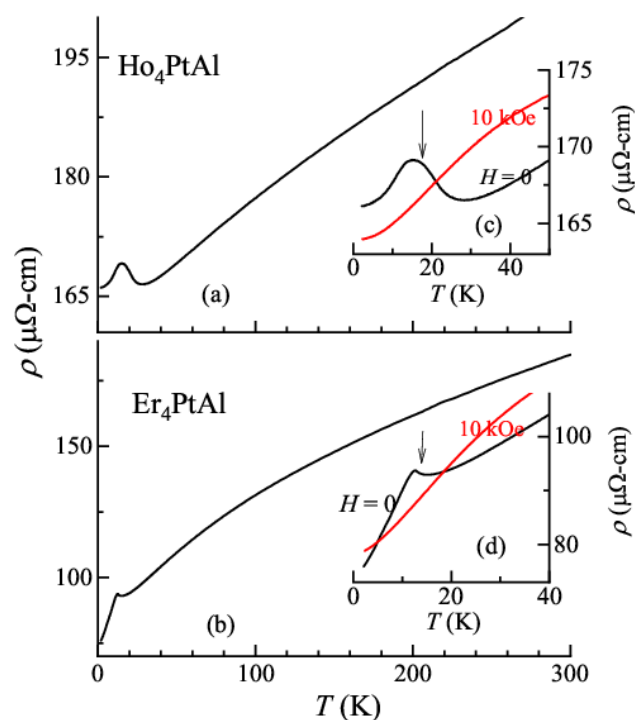
Figure 8. Zero-field electrical resistivity in the range 2–300 K are shown for Ho_4PtAl and Er_4PtAl in (**a**,**b**), respectively. The data below 50 K for the Ho case and below 40 K for the Er case in zero-field and in 10 kOe are shown in the insets c–f in an expanded form to show the existence of a resistivity minimum. Vertical arrows mark Néel temperature, inferred from other measurements presented in the text.
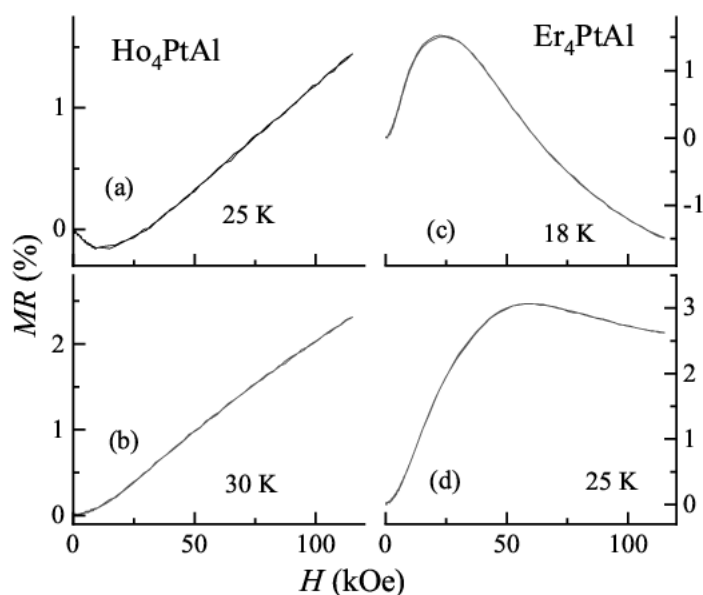

Figure 9. Isothermal magnetoresistance $[\varrho(H) - \varrho(0)]/\varrho(0)$ as a function of the magnetic field at selected temperatures above T_N; (**a**) 25 K and (**b**) 30 K for Ho_4PtAl; and (**c**) 18 K and (**d**) 25 K for Er_4PtAl.
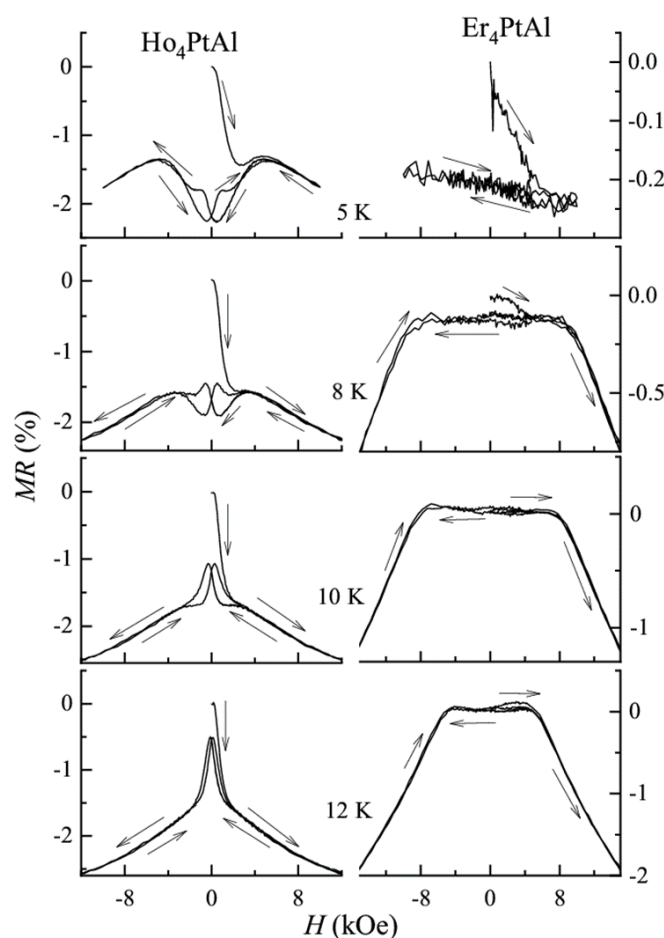
Figure 10. Magnetoresistance hysteresis loops at 5, 8, 10, and 12 K for Ho_4PtAl and Er_4PtAl.

4. Conclusions

The present results establish that Ho_4PtAl and Er_4PtAl, are interesting magnetic materials with re-entrant spin-glass behavior with the onset of magnetic order of an antiferromagnetic type, but undergoing subtle changes in this magnetic state by an application of a small external field. A notable finding is that these compounds show the largest value of isothermal entropy change (a measure of magnetocaloric effect) at the onset of magnetic order within this family, in particular with respect to the isomorphous Gd compound. Since the values surpass that of an S-state ion, this finding suggests that the topology of the $4f$ orbital can enhance the magnetocaloric effect. Another intriguing outcome, based on the comparison of the MCE behavior of Pt-based family with that of Rh family, is that Pt $5d$ spin-orbit coupling also may play a role in this regard. We hope these inferences provide clues for the advancement of theories in the field of MCE to enable the engineering of materials for magnetic refrigeration at room temperature (see, for instance, Ref. [31] for a report on thin film route of a manganite to enhance MCE with respect to Gd metal at room temperature). This entropy behavior of the Er compound meets the much-needed [27] characteristic of "reversibility" for magnetocaloric applications in the low temperature range. Finally, neutron diffraction studies would be rewarding to understand the magnetic structure changes with temperature and magnetic field in these materials.

Author Contributions: Conceptualization, E.V.S.; methodology, K.K.I. and R.K.; validation, K.K.I., R.K., K.M., and E.V.S.; formal analysis, K.K.I. and S.R.; data curation, K.K.I. and R.K.; writing—original draft preparation, K.K.I.; writing—review and editing, E.V.S., S.R. and K.M.; visualization, E.V.S.; supervision, E.V.S. and K.M.; project administration, K.M.; funding acquisition, K.M., E.V.S., S.D. and S.M. All authors have read and agreed to the published version of the manuscript.

References

1. Pecharsky, V.K.; Gschneidner, K.A. Giant Magnetocaloric effect in $Gd_5(Si_2Ge_2)$. *Phys. Rev. Lett.* **1997**, *78*, 4494–4497. [CrossRef]
2. Tappe, F.; Schwickert, C.; Linsinger, S.; Pöttgen, R. New rare earth-rich aluminides and indides with cubic Gd_4RhIn-type structure. *Monatsch. Chem.* **2011**, *142*, 1087. [CrossRef]
3. Doğan, A.; Rayaprol, S.; Pöttgen, R. Structure and magnetic properties of RE_4CoCd and RE_4RhCd (RE = Tb, Dy, Ho). *J. Phys. Condens. Matter.* **2007**, *19*, 0762131–07621313. [CrossRef]
4. Kersting, M.; Matar, S.F.; Schwickert, C.; Pöttgen, R. Segregation of Calcium and Magnesium into Different Substructures. $Ca_4Ag_{0.948}Mg$ and Other Compounds with Gd_4RhIn-type Structure. *Z. Naturforsch.* **2012**, *67*, 61–69. [CrossRef]
5. Engelbert, S.; Janka, O. RE_4TAl (RE = Y, Sm, Gd–Tm, Lu; T = Pd, Pt)—Synthesis and magnetism of new aluminum representatives with the Gd_4RhIn type structure. *Intermetallics* **2018**, *96*, 84–89. [CrossRef]
6. Kumar, R.; Sharma, J.; Iyer, K.K.; Sampathkumaran, E.V. Reentrant spin-glass and transport behavior of Gd_4PtAl, a compound with three sites for Gd. *J. Magn. Mag. Mater.* **2019**, *490*, 165515. [CrossRef]
7. Kumar, R.; Iyer, K.K.; Paulose, P.L.; Sampathkumaran, E.V. Spin-glass features at multiple temperatures and transport anomalies in Tb_4PtAl. *J. Appl. Phys.* **2019**, *126*, 123906. [CrossRef]
8. Kumar, R.; Iyer, K.K.; Paulose, P.L.; Sampathkumaran, E.V. Ferromagnetism to spin-glass transition and magnetotransport anomalies in Dy_4PtAl. *AIP Conf. Proc.* **2020**, *2265*, 030509.
9. Kumar, R.; Iyer, K.K.; Paulose, P.L.; Sampathkumaran, E.V. Competing magnetic interactions and magnetoresistance anomalies in cubic intermetallic compounds, Gd_4RhAl and Tb_4RhAl, and enhanced magnetocaloric effect for the Tb case. *Phys. Rev. Mater.* **2021**, *5*, 054407. [CrossRef]
10. Kumar, R.; Sampathkumaran, E.V. Magnetic frustration and paramagnetic state transport anomalies in Ho_4RhAl and Er_4RhAl: Possible test cases for newly identified roles of itinerant electrons. *J. Magn. Mag. Mater.* **2021**, *538*, 168285. [CrossRef]
11. Iyer, K.K.; Matteppanavar, S.; Dodamani, S.; Maiti, K.; Sampathkumaran, E.V. Magnetic behavior of cubic Dy_4RhAl with respect to isostructural Dy_4PtAl, revealing a novel $4f$ d-band interaction. *J. Magn. Magn. Mater.* **2023**, *568*, 170406. [CrossRef]
12. Buschow, K.H.J. Intermetallic compounds of rare-earths and non-magnetic metals. *Rep. Prog. Phys.* **1979**, *42*, 1373. [CrossRef]
13. Marcano, N.; Gómez Sal, J.C.; Espeso, J.I.; Fernández Barquín, L.; Paulsen, C. Cluster-glass percolative scenario in $CeNi_{1-x}Cu_x$ studied by very low-temperature ac susceptibility and dc magnetization. *Phys. Rev.* **2007**, *76*, 224419. [CrossRef]
14. Yamamoto, T.D.; Kotani, A.; Nakajima, H.; Okazaki, R.; Taniguchi, H.; Mori, S.; Terasaki, I. Ferromagnetic Cluster Glass Phase Embedded in a Paramagnetic and Metallic Host in Non-Uniform Magnetic System $CaRu_{1-x}Sc_xO_3$. *J. Phys. Soc. Jpn.* **2016**, *85*, 034711. [CrossRef]
15. Upadhyay, S.K.; Iyer, K.K.; Sampathkumaran, E.V. Magnetic behavior of metallic kagome lattices, $Tb_3Ru_4Al_{12}$ and $Er_3Ru_4Al_{12}$. *J. Phys. Condens. Matter.* **2017**, *29*, 325601. [CrossRef] [PubMed]
16. Noakes, D.R.; Shenoy, G.K. The effect of a crystalline electric field on the magnetic transition temperatures of rare-earth rhodium borides. *Phys. Lett. A* **1982**, *91*, 35–36. [CrossRef]
17. Dunlap, B.D.; Hall, L.N.; Behroozi, F.; Crabtree, G.W.; Niarchos, D.G. Crystal-field effects and the magnetic properties of rare-earth rhodium borides. *Phys. Rev. B* **1984**, *29*, 6244. [CrossRef]
18. Adroja, D.T.; Malik, S.K. Magnetic-susceptibility and electrical-resistivity measurements on $RPdSn$ (R = Ce–Yb) compounds. *Phys. Rev. B* **1992**, *45*, 779. [CrossRef]
19. Gschneidner, K.A., Jr.; Pecharsky, V.K.; Tsokol, A.O. Recent developments in magnetocaloric materials. *Rep. Prog. Phys.* **2005**, *68*, 1479. [CrossRef]
20. Li, L.; Yan, M. Recent progresses in exploring the rare earth based intermetallic compounds for cryogenic magnetic refrigeration. *J. Alloys Compd.* **2020**, *823*, 153810. [CrossRef]
21. Takayama, T.; Chaloupka, J.; Smerald, A.; Khaliullin, G.; Takagi, H. Spin-orbit entangled electronic phases in 4d and 5d transition metal compounds. *J. Phys. Soc. Jpn.* **2021**, *90*, 062001. [CrossRef]

22. Medicherla, V.R.R.; Patil, S.; Singh, R.S.; Maiti, K. Origin of ground state anomaly in LaB$_6$ at low temperatures. *Appl. Phys. Lett.* **2007**, *90*, 062507. [CrossRef]

23. Bindu, R.; Maiti, K.; Khalid, S.; Sampathkumaran, E.V. Structural link to precursor effects. *Phys. Rev. B* **2009**, *79*, 094103. [CrossRef]

24. Bindu, R.; Adhikary, G.; Sahadev, N.; Lalla, N.P.; Maiti, K. Pseudogap and charge ordering in a large-bandwidth electron-doped manganite. *Phys. Rev. B* **2011**, *84*, 052407. [CrossRef]

25. 25. Maiti, K; Singh, R.S.; Medicherla, V.R.R.; Rayaprol, S.; Sampathkumaran, E.V. Origin of charge density wave formation in insulators from a high resolution photoemission study of BaIrO$_3$. *Phys. Rev. Lett.* **2005**, *95*, 016404. [CrossRef]

26. Chaudhary, V.; Chen, X.; Ramanujan, R.V. Iron and manganese based magnetocaloric materials for near room temperature thermal management. *Prog. Mater. Sci.* **2019**, *100*, 64–98. [CrossRef]

27. Law, J.Y.; Moreno-Ramirez, L.M.; Diaz-Garcia, A.; Franco, V. Current perspective in magnetocaloric materials research. *J. App. Phys.* **2023**, *133*, 040903. [CrossRef]

28. Mallik, R.; Sampathkumaran, E.V. Magnetic precursor effects, electrical and magnetoresistance anomalies, and heat-capacity behavior of Gd alloys. *Phys. Rev. B* **1998**, *58*, 9178. [CrossRef]

29. Kumar, R.; Iyer, K.K.; Paulose, P.L.; Sampathkumaran, E.V. Magnetic and transport anomalies in R_2RhSi$_3$ (R = Gd, Tb, and Dy) resembling those of the exotic magnetic material Gd$_2$PdSi$_3$. *Phys. Rev. B* **2020**, *101*, 144440. [CrossRef]

30. Wang, Z.; Barros, K.; Chern, G.-W.; Maslov, D.L.; Batista, C.D. Resistivity Minimum in Highly Frustrated Itinerant Magnets. *Phys. Rev. Lett.* **2016**, *117*, 206601. [CrossRef]

31. Zhao, B.; Hu, X.; Dong, F.; Wang, Y.; Wang, H.; Tan, W.; Huo, D. The magnetic properties and magnetocaloric effect of Pr$_{0.7}$Sr$_{0.3}$MnO$_3$ thin film grown on SrTiO$_3$ substrate. *Materials* **2023**, *16*, 75. [CrossRef] [PubMed]